Wavelet-Based Analysis of Lower Hybrid Full-Wave Fields*)

Orso MENEGHINI[a)], Syunichi SHIRAIWA and Ronald PARKER

Massachusetts Institute of Technology, Cambridge MA, USA

(Received 10 December 2011 / Accepted 18 June 2012)

In this paper, we introduce the use of Continuous-Wavelet-Transform (CWT) to postprocess full-wave fields of Lower Hybrid (LH) waves which have been generated using the LHEAF code. Compared to the Fourier transform, the CWT has the appealing property of yielding information as to the spatial location of spectral modes. Using a complex-Morlet CWT, the complicated full-wave field pattern is decomposed into its spectral components parallel to the static magnetic field $n_\parallel$. In general, the CWT of the LHEAF full-wave fields shows that the local wave spectrum broadens as the waves propagate through the plasma and after reflection off the low density cutoff or the vacuum vessel walls. The goal of this analysis is to provide a tool to assess the importance of full-wave effects on the transformation of the wave $n_\parallel$ spectrum which governs the LH power absorption and driven currents.

Keywords: LHEAF, Lower Hybrid, Alcator C-Mod, LHCD, Morlet

DOI: 10.1585/pfr.7.2403111

1. Introduction

The dynamics of Lower Hybrid (LH) waves in a plasma is well understood in therms of the evolution of their $n_\parallel$ spectrum. In full-wave methods the information about the local $n_\parallel$ wave spectrum is not readily available as in ray-tracing codes and must be recovered from the wave fields.

Based on the experience built upon ray-tracing codes, one may expect certain spectral components to be spatially localized, at least for the cases when stochastic effects are unimportant [1]. In mathematical terms that is to say the wave fields are non-stationary along a flux surface.

Fourier transform of the parallel wave fields along the field lines can provide insight into what spectral components exist on flux surfaces, however it does not provide any information about their spatial localization. Instead, the Continuous Wavelet Transform (CWT) can be used decompose the complicated full-wave field patterns into its local $n_\parallel = c\,k_\parallel/\omega$ spectral components along a field line.

A similar analysis was first described in Ref. [2], for the visualization of dispersion, amplitude and wave polarization information of full-wave fields in the context of full-wave ICRF mode-conversion simulations in 1D. In this paper the LH full-wave fields from the LHEAF code [3, 4] are analyzed.

2. Wavelet Analysis Formalism

To first approximation, a Wavelet Transform (WT) can be thought of as technique to extract the spectrogram of a signal. As in Windowed Fourier Transform (WFT), a signal spectrum is Fourier analyzed in segments of size x_w, each small enough for the portions of the signal to be assumed stationary. However, unlike the WFT, which uses a constant x_w for all frequencies, the WT analyzes each frequency component with a x_w matched to its scale. In other words, the WT is designed to have good spatial but poor spectral resolution for high frequency components, and viceversa for low frequency components. This approach minimizes two conflicting types of errors: the *Heisenberg error*

$$\Delta k_H \propto \frac{1}{x_w}, \tag{1}$$

and the *gradients error*

$$\Delta k_\nabla = \frac{\partial k}{\partial x} x_w, \tag{2}$$

over a wide range of frequency components, under the assumption that long wavelength variations occur on a scale length which is longer than the one of short wavelength variations, as it is often the case in physical systems.

2.1 Wavelet transform

The wavelet transform of a signal $f(x)$ is obtained by convolving such signal with a finite support function $\Psi(x)$ (named *wavelet*) and taking the Fourier transform at each step of the convolution:

$$C(x,\alpha) = \int_{-\infty}^{\infty} f(x') \frac{1}{\sqrt{\alpha}} \Psi^\star \left(\frac{x'-x}{\alpha} \right) \mathrm{d}x' \,. \tag{3}$$

Alternatively, the same operations can be interpreted as a set of filtering operations in spectral space

$$C(x,\alpha) = \frac{1}{\sqrt{2\pi}} \int_{-\infty}^{\infty} \hat{f}(k)\, \sqrt{\alpha}\, \hat{\Psi}^\star(\alpha\, k) \exp^{ikx} \mathrm{d}k, \tag{4}$$

author's e-mail: meneghini@fusion.gat.com

a) Present address; General Atomics, San Diego, CA 92186, USA

*) This article is based on the presentation at the 21st International Toki Conference (ITC21).

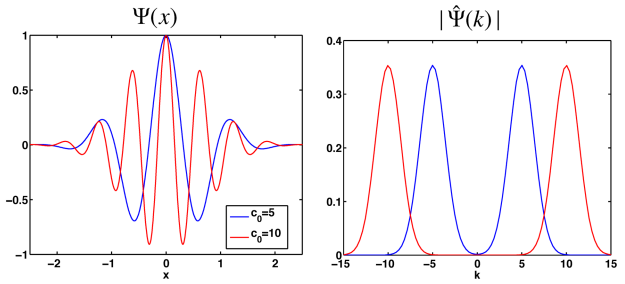

Fig. 1 Morlet wavelet and its Fourier transform (magnitude) plotted for two different values of the parameter c_0. The parameter c_0 can be used to adjust the ratio between the errors Δk_H and Δk_∇.

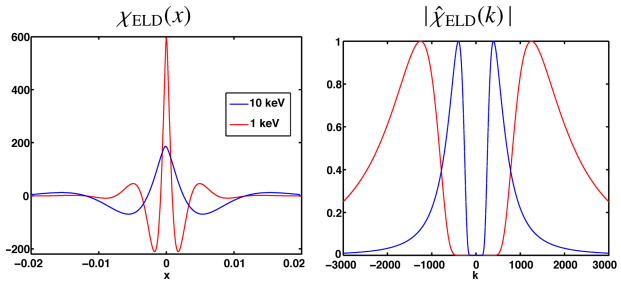

Fig. 2 Imaginary susceptibility arising from Electron Landau Damping (ELD) for a Maxwellian plasma in real and spectral domains for two different electron temperatures.

where $\hat{\Psi}(k)$ is the Fourier transform of the function $\Psi(x)$ (i.e. the filter transfer function) and $\hat{f}(k)$ is the spectrum of $f(x)$.[1]

Here the parameter α is used to dilate the support x_w of the wavelet function such that $x_w \propto 1/k$. By this approach, the Heisenberg error relative to each spectral component $\Delta k_H/k$ is kept constant and the gradients error relative to each spectral component equals $\Delta k_\nabla/k = (\partial k/\partial x)/k^2$, which one may recognize as the adiabatic-change criteria of the WKB theory [5]. Imposing the errors to be equal $\Delta k_\nabla = \Delta k_H$ results in $c = (\partial k/\partial x)/k^2$ which in practice sets a condition on the wavelet function used, depending on how well the adiabatic-change criteria is satisfied in the system under consideration.

The CWT is an implementation of the WT using which uses arbitrary scales α; these wavelets do not form an orthogonal basis, meaning that data at different locations and frequencies are correlated to each other.

2.2 Complex morlet wavelet

The Morlet wavelet is defined as a sinusoidal signal multiplied by a Gaussian envelop. Plots of the Morlet wavelet in real and spectral space are shown in Fig. 1. In the following it's complex analogue is used to sample the signal for either its positive or negative k components:

$$\Psi(x) = \exp(-x^2 \pm i\, c_0\, x)\,. \tag{5}$$

The Full-Width Half Maximum FWHM of the Morlet wavelet power spectrum is $\Delta k_H = 2\sqrt{\log(2)}$. As the spectrum is centered at $k = c_0$, the spectral accuracy at every wavelet scale is $\Delta k_H/k \approx 1.66/c_0$. The parameter c_0 can therefore be used to control the ratio between the Heisenberg and the gradient error. Satisfying the WKB and the eikonal wavenumber conditions requires $kL \gg kx_w = c_0 \gg 1$, where L is the scale-length that one wants the CWT to resolve for a given k.

Worth pointing out is that the Morlet wavelet resembles very closely to the imaginary susceptibility arising from Electron Landau Damping (ELD) for a Maxwellian plasma $\chi_{\mathrm{ELD}}(x)$, shown in Fig. 2 [3]. This suggests that is possible to interpret $\chi_{\mathrm{ELD}}(x)$ as a wavelet whose support scales depending on the plasma temperature, thus selecting specific spectral $k_\parallel$ components with which the waves interact.

[1] Numerically, the latter approach is preferred in view of the numerical efficiency of the Fast Fourier Transform (FFT) algorithm $O(N \log N)$ compared to a numerical convolution $O(N^2)$.

3. Simulation Results of an Alcator C-Mod LHCD Discharge Using LHEAF

Figure 3 shows the wave parallel electric field $E_\parallel$ from a LHEAF simulation of an Alcator C-Mod LHCD discharge ($B = 5.4\,\mathrm{T}$, $\bar{n}_\mathrm{e} = 1.3 \times 10^{20}\,\mathrm{m}^{-3}$, $\sim 600\,\mathrm{kW}$ of net power with launched $n_{\parallel,\mathrm{ant}} = 1.9$) both in phase [6] and real space. In the plots, the arrows represents the trajectory of the same ray-tracing calculation, and is intended to be used as a guideline on how to interpret the full-wave result.

In real-space, one sees four waveguide rows injecting RF power into the plasma from the low field side of Alcator C-Mod cross-section. Once the waves propagate through the SOL, they become quickly electrostatic and propagate in the form of resonance cones, making small angles with respect to the static magnetic field. After propagating through the plasma, the waves undergo reflection either at a cutoff layer or at the vacuum vessel walls. In the vicinity of the locus of closest approach to the plasma core, the waves resonance cones are observed to fann-out. Finally, though week in amplitude, one can observe spiral-like structures close to the center of the plasma which are associated with the formation of caustics.

The phase-space plot shows the $E_\parallel$ power spectrum as a function of normalized wave phase parallel velocity $v_\parallel/c = 1/n_\parallel$ and normalized minor radius $\rho = r/a$. In this plot the wave fields are mostly confined in the region of velocity space lying between the slow-wave accessibility condition $v_{\parallel,\mathrm{acc}}$ (dashed black-white line) and the $3\,v_{T_\mathrm{e}}$ boundary (dashed red-black line), where the waves are strongly damped due to ELD. Following the arrow, one sees that the waves enter the separatrix with $v_\parallel/c \sim 2$ and first downshift until they reach a point of minimum approach to the plasma core, which occurs in the vicinity of

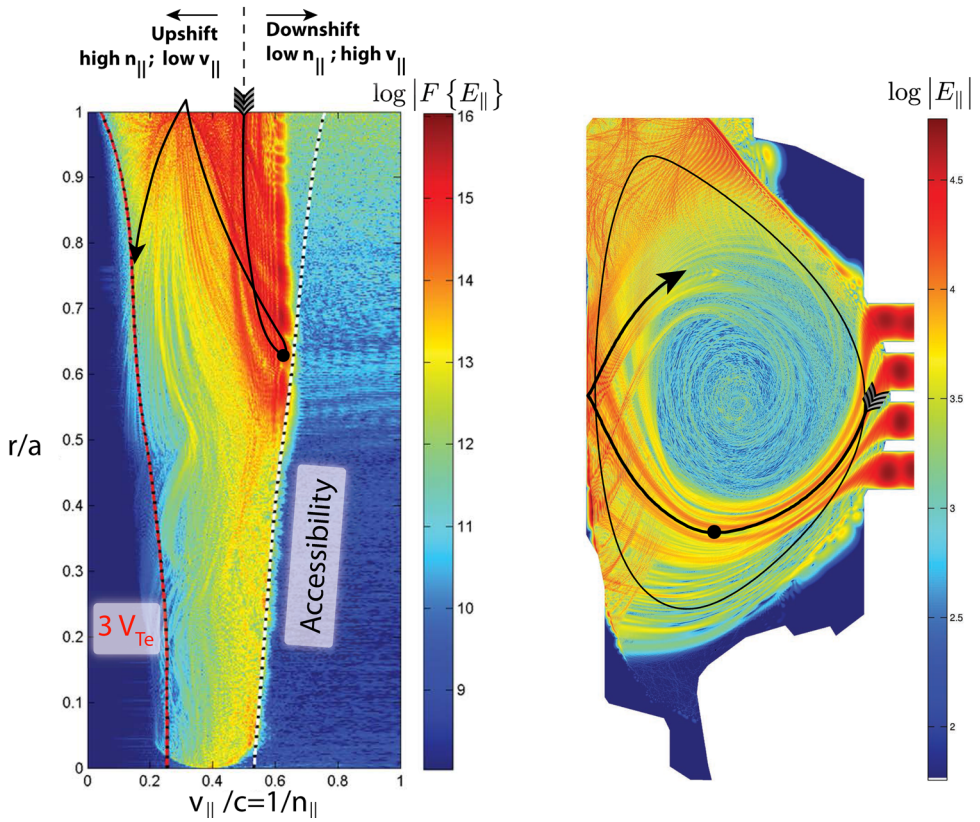

Fig. 3 Full-wave solution in phase (left) and real space (right) of an Alcator C-Mod LHCD discharge simulated in LHEAF.

the slow-fast wave confluence point. The waves then upshift as they propagate back towards the plasma edge, cross the separatrix, reflect in the SOL and are finally damped around $3\,v_{T_e}$.

Figure 4 shows the wavelet transform of the wave fields in the core of the plasma, plotted as a function of $n_\parallel$. In this figure, the parameter c_0 of the Morlet wavelet was set to 20, as it results in a good tradeoff between spectral and spatial resolution of the wavelet decomposition. The spectral resolution is $\Delta n_\parallel/n_\parallel = 0.083$ and is smaller than separation among the $n_\parallel$ frames of Fig. 4. For the Alcator C-Mod wave frequency of 4.6 GHz, the spatial resolution along the field lines is $\sim 20\,\mathrm{cm}/n_\parallel$. Considering a maximum field line pitch angle of ~ 10 deg on the low field side edge of the plasma, this corresponds to a cross-sectional spatial resolution of $\sim 4\,\mathrm{cm}/n_\parallel$. Hence, for LH waves with $n_\parallel \gtrsim 2$, the spatial resolution is at least one order of magnitude smaller than the plasma minor radius $a = 22$ cm.

Since the $n_\parallel$ spectrum changes continuously along the wave propagation, up or down shifting of the spectrum can be studied by tracking the evolution of the wavelet power spectrum peaks across different $n_\parallel$ frames. The spectral broadness instead can be estimated by counting for how may $n_\parallel$ frames does a feature persists at the same physical location in the plasma.

To confirm the analysis carried out in Fig. 3, indeed the waves which enter the low-field-side of the separatrix with $n_\parallel \approx 2.0$, first downshift ($n_\parallel < 2.0$) and subsequently upshift ($n_\parallel > 2.0$). Also, the slow- fast- wave confluence point at $v_{\parallel,\mathrm{acc}}$ (dashed black-white line) shows which region of the plasma is accessible for waves with a given $n_\parallel$. The waves which are circumscribed by the line are inaccessible. Similarly, inside of the $3\,v_{T_e}$ boundary (dashed red-black line) the waves are strongly damped by ELD.

Broad spectral features associated with strong $n_\parallel$ upshift are observed after the waves reflect off the inner wall and the upper divertor region. Strong changes of the $n_\parallel$ spectrum in these region are expected, since the reflecting surfaces are not aligned with the static magnetic field. This analysis also highlights the presence of spiral-like structures near the center of the plasma which are associated with the formation of caustics. Here, the waves clearly spiral around or just outside of the magnetic axis, depending on their $n_\parallel$ and the wave fields are excluded from this region for all $n_\parallel$ but in the vicinity of $n_\parallel = n_{\parallel,\mathrm{ant}} R_0/(R_0 + a) \approx 2.6$ (here $R_0 = 0.67$ cm and $a = 0.24$ cm). This is the "whispering gallery effect" which is also observed in ray-tracing [7] and beam-tracing [8] simulations and is the result of LHEAF being a single toroidal mode number simulation.

Certainly, like in ray-tracing calculations, one of the driving mechanism behind the waves upshift are the variations in the poloidal and radial wave number which are associated with a toroidal geometry [9] and a strongly shaped plasma. Nonetheless, the spectral broadening observed in LHEAF is larger than the one predicted by ray-

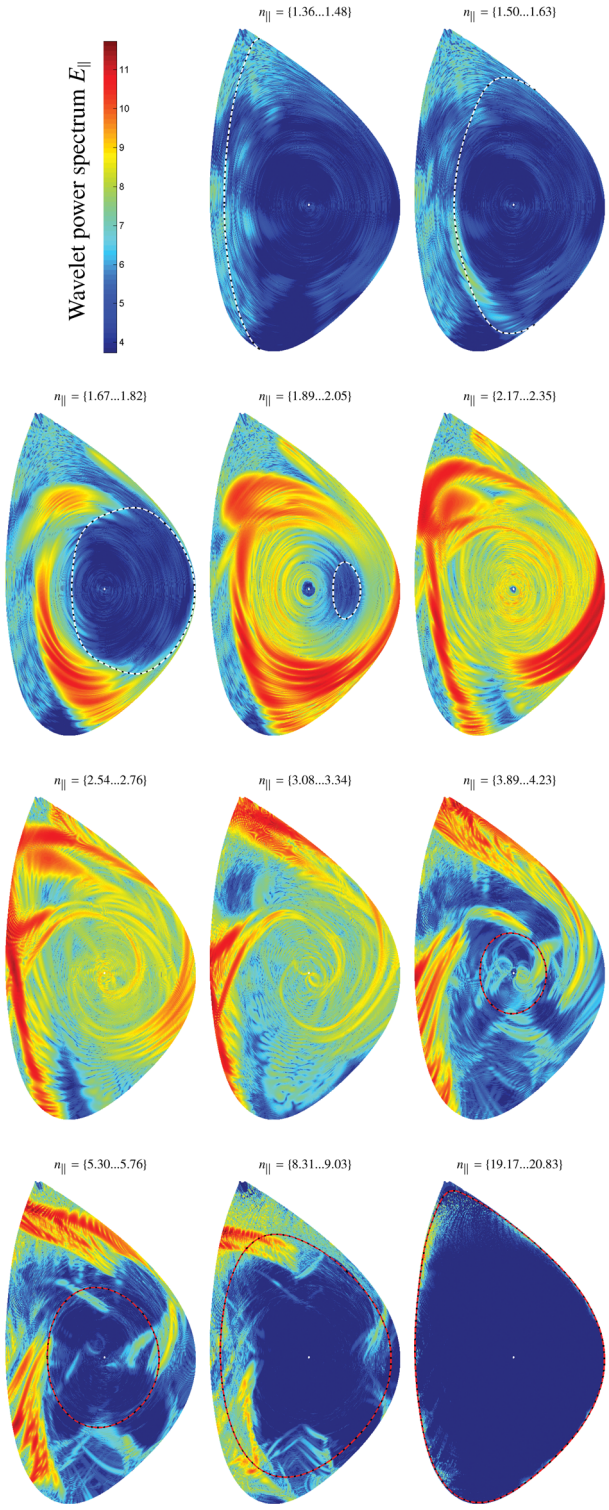

Fig. 4 Logarithmic plots of a set of $E_\parallel$ wavelet power spectra equispaced in $v_\parallel/c = 1/n_\parallel$ and normalized to the same absolute magnitude. The full-width half maximum of the wavelet power spectrum is printed as an $n_\parallel$ range on top of each frame. White-black and red-black dashed lines represents the accessibility and the $3\,v_{T_e}$ boundaries, respectively.

tracing codes [6] and full-wave effects have been proposed as a mechanism that could explain such strong upshift. In particular at the slow-fast wave confluence point, caustics and cutoffs the WKB approximation is likely to be violated, since whenever the transverse dimension of the LH resonance cone is comparable to the perpendicular wavelength, wave diffraction becomes significant and the waves are blurred both in real and spectral space [8].

4. Conclusions and Future Work

This paper introduces the use of CWT to decompose LH full-wave fields into its constituent $n_\parallel$ components and obtain information about the waves local $n_\parallel$ spectrum. Such information is critical to understand the full-wave solution (wave propagation, absorption and current drive performance), especially in the multipass-absorption regime, where multiple waves with different wavelengths are present simultaneously. Future work will be focused at comparing the local parallel wavenumber information between the full-wave and the ray/beam-tracing simulations, with the aim of investigating the role of full-wave effects and the origin of the strong spectral broadening which is observed in LHEAF simulations.

Supported by U.S. DoE grants DE-FC02-99ER54512 and DE-AC02-76CH03073

[1] K. Kupfer, D. Moreau and X. Litaudon, Phys. Fluids B: Plasma Physics **5**, 4391 (1993).
[2] D.A. D'Ippolito, J.R. Myra, E.F. Jaeger, L.A. Berry and D.B. Batchelor, AIP Conference Proc. **694**, 463 (2003).
[3] O. Meneghini, S. Shiraiwa and R. Parker, Phys. Plasmas **16**, 090701 (2009).
[4] S. Shiraiwa, O. Meneghini, R. Parker, P. Bonoli, M. Garrett, M.C. Kaufman, J.C. Wright and S. Wukitch, Phys. Plasmas **17**, 056119 (2010).
[5] A. Cardinali, L. Morini, C. Castaldo, R. Cesario and F. Zonca, Phys. Plasmas **14**, 112506 (2007).
[6] S. Shiraiwa, J. Ko, O. Meneghini, R. Parker, A.E. Schmidt, S. Scott, M. Greenwald, A.E. Hubbard, J. Hughes, Y. Ma *et al.*, Phys. Plasmas **18**, 080705 (2011).
[7] M. Brambilla and A. Cardinali, Plasma Phys. **24**(10), 1187 (1982).
[8] G.V. Pereverzev, Nucl. Fusion **32**(7), 1091 (1992).
[9] P.T. Bonoli and E. Ott, Phys. Fluids **25**, 359 (1982).